Synthesis of CA_6/AlON Composites with Enhanced Slag Resistance

Yunsong Liu
University of Science and Technology Beijing
Enhui Wang
University of Science and Technology Beijing
Linchao Xu
University of Science and Technology Beijing
Tao Yang
University of Science and Technology Beijing
Xinmei Hou (houxinmei01@126.com)
University of Science and Technology Beijing
Zhijun He
University of Science and Technology Liaoning
Tongxiang Liang
JiangXi University of Science and Technology

Research Article

Keywords: CA6/AlON composite, two-step method, slag resistance

Posted Date: February 5th, 2021

DOI: https://doi.org/10.21203/rs.3.rs-184922/v1

Abstract

Aiming to improve the slag resistance of calcium hexaaluminate (CA_6), different amounts of AlON have been introduced into CA_6 using two approaches, *i.e.* one-step and two-step methods. The results show that both the two phases of CA_6 and AlON are uniformly distributed when sintered at 1650 °C for 2 h in flowing nitrogen using two-step method. The optimized amount of AlON addition is determined to be 10 wt%. In addition, the reaction test method is performed and CA_6/AlON composite exhibits much better slag penetration and corrosion resistance compared with pure CA_6. The effect of AlON is also discussed.

1 Introduction

Calcium hexaaluminate ($CaAl_{12}O_{19}$, usually denoted as CA_6) is of great interest as high temperature ceramics benefiting from the combination of excellent properties including high melting point, good alkaline resistance, high stability in a reducing atmosphere, and low thermal conductivity, and so on [1–4]. However, CA_6 possesses a magnetoplumbite structure and belongs to hexagonal crystal system (space group P63/mmc) [5–7]. This specific structure tends to result in the anisotropic growth of CA_6 grains forming the platelet shape, which is harmful to the sintering of CA_6. As a result, the obtained CA_6 usually possess more than 20% porosity even sintered at the temperature up to 1750°C [8, 9]. This structure accelerates the penetration and corrosion rate of molten slag when used as furnace lining and thus greatly limits the practical application [10, 11].

It is well known that the addition of second phase is a practicable approach to increase the densification of matrixes during the sintering process [11–15]. For instance, Yao *et al.* [13] introduced 20wt% SiO_2 into Cr_2O_3 during the sintering process in a buried carbon atmosphere. The results showed that the crystal growth of Cr_2O_3 is significantly limited and the densification of bulk composites is increased to a large extent. Luo *et al.* [14] put forward that MnO_2 can improve the densification of $Ca_2Mg_2Al_{28}O_{46}$ ceramic and the apparent porosity is decreased to 8.4% with 3 wt% MnO addition. Xu *et al.* [11, 15] found that ZrO_2 and TiO_2 can greatly decrease the porosity and pore sizes of $MgAl_2O_4$-$CaA_{l4}O_7$-$CaAl_{12}O_{19}$ composite, thereby improving the slag resistance of the composite.

$Al_{23}O_{27}N_5$ (usually denoted as AlON) as a solid solution of Al_2O_3 and AlN belongs to cubic crystal system (space group Fd-3m) [16]. Different from CA_6 in the shape of plate with a relatively big size, AlON always exists in small cubic or near-spheroidal structures. The specific structure of AlON makes it possible to fill the voids forming among CA_6 grains. Meanwhile, AlON possesses the characteristics of nitrogen oxide and it has poor wettability with metal and oxide melts [16–20]. It has been reported that AlON as the additive can improve the slag resistance of the matrix [21, 22]. Furthermore, there is no significant solid solution between CA_6 and AlON even sintered at 1750°C, which is conducive to the maintenance of respective excellent characteristics [23]. Based on this, it is reasonably to anticipate that AlON should be a promising candidate for the improvement of densification and slag resistance of CA_6.

In this study, CA_6/AlON composites have been prepared using both one-step method and two-step method for the first time. The former is directly sintered using Al_2O_3, $CaCO_3$ and Al with different ratio as raw materials in nitrogen. The latter consisting of the pre-synthesized CA_6 and AlON is sintered at 1650 ℃. The obtained CA_6/AlON composites were characterized using XRD, SEM combined with EDS. The bulk density and apparent porosity were also measured. Based on this, the slag penetration and corrosion resistance of CA_6/AlON composites was carried out. The same experiment was also conducted using pure CA_6 as the control group. The effect of AlON on the slag resistance of CA_6/AlON composites was also discussed.

2 Experimental Procedure

2.1. Raw materials

The main raw materials used in this work were analytically pure Al_2O_3, $CaCO_3$, MgO and SiO_2 powders (Sinopharm Chemical Reagent Co., Ltd., 99 wt% purity, average grain size < 44 μm), together with Al fine powders (Shanghai Aladdin Reagent Co., Ltd., 99 wt% purity, average grain size≈58 μm). Aiming to guarantee the validity for synthetic samples, Al_2O_3, SiO_2 and MgO powders before use were calcined to 1000 ℃ for 1 h in a muffle furnace to remove the absorbed water and bound water.

2.2. Preparation of CA_6/AlON composites

2.2.1 One-step method

In view of one-step method, the pre-fired Al_2O_3 and $CaCO_3$ powders as well as Al powder with different proportions were wet ball-milled for 24 h using absolute ethanol as medium. The resulting slurry was dried in a vacuum drying cabinet at 100 ℃ for 12 h, grounded in a mortar, and filtrated through nylon sieves with the screen mesh of 120. Subsequently, the obtained mixture was pressed under 20 MPa into 25 mm × 25 mm cylinders. Finally, the specimens were sintered at the temperature range from 1650°C to 1750°C for 3 h under flowing nitrogen atmosphere.

2.2.2 Two-step method

As for two-step method, it mainly includes the preparation of single CA_6 and AlON phases and the sintering process of CA_6/AlON composites. Regarding the preparation of AlON phase, aluminothermic reduction nitridation method was herein adopted [24–26]. Firstly, the pre-fired Al_2O_3 and Al powders were weighed at a mass ratio of 88:12. Then the mixture was wet milled for 24 h and dried in vacuum at 100 ℃ for 10 h. Afterwards, the dried powder mixture was pressed into a 50 mm block under a pressure of 30 MPa and then sintered at 1750°C in a graphite crucible for 3 h under flowing N_2 atmosphere. Eventually, the AlON ceramic block was pulverized using 200–300 mesh to obtain AlON powder for later use. Likewise, the single CA_6 phase was also prepared using pre-fired Al_2O_3 and $CaCO_3$ as raw materials and sintered at 1550 ℃ for 2 h in air. The resulting CA_6 block was further crushed to obtain CA_6 powders with

similar size range as AlON powder. During the synthetic process of CA_6/AlON composite, AlON and CA_6 powders obtained above were further mixed, ball milled, dried, pressed, and then sintered at 1650°C for 2 h in flowing nitrogen atmosphere.

It should be pointed out that the amount of AlON incorporated during the above two methods were 5 wt%, 10 wt%, 15 wt% and 20 wt%. For simplicity, CA_6/AlON composites prepared by one-step method and two-step method were named as SI-*x* and SII-*x* respectively, where *x* denotes the amount of AlON as shown in Table 1.

Table 1
Composition of the designed CA_6/AlON composites (wt%).

Composites prepared by one-step method	Composites prepared by two-step method	CA_6	AlON
SI-5	SII-5	95	5
SI-10	SII-10	90	10
SI-15	SII-15	85	15
SI-20	SII-20	80	20

2.3. Slag penetration and corrosion test

The reaction test method as shown in Fig. 1 was adopted to evaluate the slag penetration and corrosion resistance of CA_6/AlON composites [10, 11, 27]. This method has two main purposes. One is to assess the wettability between the molten slag and the matrix. The second is to provide an intuitive way to observe the coupled penetration and corrosion effect of molten slag on the matrix. Herein, the typical refining ladle slags as illustrated in Table 2 were pressed into cylinders with 30 mm in diameter and 5 mm in height. The slag cylinders were then put on the polished surfaces of CA_6/AlON composite and pure CA_6 matrixes with approximate 30 mm in height respectively, followed by the reaction test in a chamber electric furnace with carbon buried at 1550 ℃ for 0.5 h. After cooled down to room temperature, they were cut perpendicularly to the slag-matrix interface and polished. The dimensional changes of CA_6/AlON composite and pure CA_6 matrixes before and after the reaction test and the penetration depth of the slag were evaluated.

Table 2
Chemical composition of model slag (wt%).

Oxides	CaO	Al_2O_3	SiO_2	MgO	C/S
Contents	59.1	19.3	17.3	4.3	3.42

2.4. Characterization

The crystalline phases of the synthesized samples were examined by the X-ray diffraction (XRD) analyzer (Cu Kα radiation, MAC Science Co. Ltd., Japan) from 10° to 90° at a step of 0.02°. The surface and cross-section morphologies as well as chemical analysis of the samples were characterized by a scanning electron microscopy (SEM, JSM-840A, JEOL, Japan) in combination with energy dispersive X-ray spectrometry (EDS). In addition, the bulk density and apparent porosity were evaluated in terms of the Archimedes law.

3 Results And Discussion

3.1 Preparation and characterization of CA_6/AlON composites by one-step method

Figure 2 shows the typical XRD patterns of SI-10 prepared by one-step method at different sintering temperatures. It can be seen that the main phase of the sample sintered at 1650°C is CA_6 with a small amount of Al_2O_3 and AlN. When the temperature rises up to 1700°C, new characteristic peaks corresponding to AlON can be observed. Meanwhile, the relative intensities of the characteristic peaks of Al_2O_3 are significantly reduced, indicating that higher sintering temperature can enhance the solid-solid reaction of Al_2O_3 and AlN to form AlON. This phenomenon is well consistent with the results reported in the literatures [24, 28]. With the sintering temperature further increasing to 1750°C, the main phases of the sintered products transform into CA_6 and AlON. The phase evolution for SI-5, SI-15 and SI-20 is almost the same to SI-10, therefore they are herein not described for brevity.

The fracture morphologies of CA_6/AlON composite sintered at 1750°C using one-step method are further observed. The representative SEM images of SI-10 and SI-20 are illustrated in Fig. 3. It can be seen from Fig. 3(a) that the SI-10 are composed of two typical morphologies, *i.e.* plate structures with relatively big size and clusters with relatively small size. Combined with EDS analysis, they are determined to be CA_6 and AlON as marked by the red dotted line. The reason for the formation of AlON clusters should be closely related to the cluster characteristic of Al powders with a low molten point of 659°C. During the sintering process, the liquid Al has bad wettability on Al_2O_3, so it will tend to aggregate and precipitate on the surface of Al_2O_3. Then, these liquid tiny AlN droppings can be further nitridized into fine AlN particles with high activity [24, 26]. When the temperature further increases up to the critical point where the reaction between AlN and Al_2O_3 start to occur, AlON phase is generated in situ and gradually form AlON clusters as marked in Fig. 3. When the amount of AlON is increased up to 20 wt%, the morphology of SI-20 is nearly unchanged, except that more AlON clusters are formed as shown in Fig. 3(b). In addition, it should be noted that the porosity of CA_6/AlON composites is rather high and is not decreased even more AlON is added. Therefore, it is reasonably to conclude that one-step method is not an appropriate approach to prepare dense CA_6.

3.2 Preparation and characterization of CA_6/AlON composites by two-step method

3.2.1 Preparation of single CA_6 and AlON phases

Figure 4 illustrates the XRD pattern and fracture SEM image of single CA_6 phase sintered at 1550 ℃ for 2 h in air. It can be seen from Fig. 4(a) that the predominant peaks correspond well to CA_6 phase (JCPDS: No. 76–0665), confirming the high purity of obtained CA_6. In view of the fracture microstructure, CA_6 grains exhibit hexagonal plate and porous structure.

XRD and SEM analysis of single AlON phase sintered at 1750 ℃ for 2 h in flowing nitrogen atmosphere are shown in Fig. 5. Figure 5(a) shows that the obtained AlON phase (JCPDS: No. 80-2171) possesses good crystalline character and high purity. From Fig. 5(b), it can be found that the AlON grains are in relatively small size and evenly distributed.

3.2.2 Preparation of CA_6/AlON composites

CA_6/AlON composites with different amounts of AlON addition have been prepared according to the procedures provided in Sect. 2.2.2 and the corresponding fracture SEM images are shown in Fig. 6. It can be found from Fig. 6(a) that the grains are evenly distributed in the fracture surface. Combined with the enlarged view (Fig. 6(b)) and EDS analysis, small AlON grains are uniformly distributed around the big CA_6 grains. When the amount of AlON is added up to 10 wt% (Figs. 6(c) and (d)), the porosity in SII-10 is obviously decreased. The newly added AlON should fill the voids between CA_6 grains and thus increases the densification. However, the further decrease in porosity is not obvious in SII-15 and SII-20 with more AlON addition (Figs. 6(e)-(h)). This phenomenon may be attributed to the fact that some excessive AlON grains can distribute on the surface rather than the voids between CA_6 grains, which in turn increases the porosity of the composites.

To quantify the effects of AlON addition on CA_6/AlON composites, bulk density and apparent porosity have been further characterized as depicted in Fig. 7. It can be seen that with the amount of AlON increasing, the bulk density and apparent porosity gradually increase and decrease, respectively. Besides, the changing trends are much more obvious when AlON addition is below 10 wt%. The bulk density and apparent porosity are 2.26 $g \bullet cm^{-3}$ and 20.2%, respectively. When more AlON is added (SII-15 and SII-20), there are small amplitude of changes especially for apparent porosity. From the above results, the optimized amount of AlON in CA_6/AlON composites is determined to be 10 wt% with the consideration of relatively high synthetic cost of AlON. It should be stated that the densification of CA_6/AlON composites can be further increased at higher temperature or using hot pressing. In this work, we mainly focus on the composite powder. More work will be carried out in the future.

3.3 Slag penetration and corrosion test

Figure 8 shows the slag penetration and corrosion test results of SII-10 with carbon buried at 1550°C for 0.5 h. For comparison, the corresponding test for pure CA_6 has also been performed. As shown in Figs. 8(a) and 8(c), the contacting surface between pure CA_6 and the slag is completely corroded and penetrated, with no slag remaining on the upper surface (Fig. 8(e)). By comparison, SII-10 exhibits a bad wettability with the molten slag (Fig. 8(b)) and some flowing slag can be observed on the side surface (Fig. 8(d)). This phenomenon should be attributed to the intrinsic character of AlON, which can increase the interfacial tension between the molten slag and SII-10 and thus increase the wetting angle [16–20]. In addition, Fig. 8(f) suggests that there is no slag penetration. A clear slag layer can be seen on the upper surface of SII-10, indicating the better slag penetration and corrosion resistance.

To further investigate the promoted mechanism of AlON addition on the slag penetration and corrosion resistance, the typical back-scattered electron (BSE) analysis of the cross-sections of pure CA_6 and SII-10 has been compared as shown in Fig. 9 and Fig. 10, respectively. Figure 9(a) shows the EDS maps for the cross sections of pure CA_6 after the slag penetration and corrosion test. It can be seen that there is no obvious boundary between the corrosion zone and unaltered matrix. From the enlarged image (Fig. 9(b)) in combination with EDS analysis, the corrosion zone is composed of CA_6 and $CaO•2Al_2O_3$ (CA_2) that distribute crossly. The absence of Si and Mg elements is resulted from the relatively low proportions in slag (Table 2), which should exist in the upper part of the corrosion zone. Figure 9(c) shows the unaltered matrix is CA_6 with high porosity. If given more slag and longer testing time, the molten slag is expected to further penetrate and corrode with the matrix.

Figure 10 shows the BSE images and corresponding element distributions of cross sections of SII-10 after slag penetration and corrosion test. The cross section (Fig. 10(a)) can be clearly divided into three parts, *i.e.* slag layer, corrosion zone and unaltered matrix. In view of the slag layer as shown in Fig. 10(b), it is confirmed by EDS analysis that the darkest areas are pores filled by carbon. In addition, some low-melting-point phases including $CaMgAl_2SiO_7$ (CMAS) and $Ca_2Al_2SiO_7$ (C_2AS) together with some high-melting-point phases consisting of CA and CA_2 as well as $MgO•Al_2O_3$ (MA) can be also observed, which is consistent with the results reported by Chen *et al.* [1] As for the corrosion zone, the thickness is approximate 345 μm. The whole phase composition in this zone is similar, *i.e.* CA_2 and C_2AS represented by pale and bright areas respectively (Figs. 10(c) and (d)). The differences lie in the following two points. Firstly, there is a gradient distribution of C_2AS phase along the corrosion direction. Secondly, CA_2 phase close to the unaltered matrix is more dense and continuous. These results suggest that CA_2 layer can effectively slow down the penetration of low-point-melting phase and thus hinder the further corrosion.

The reaction between the molten slag and the matrix is a process accompanied with the ion diffusion. According to the ionic structure model for the molten slag [29], the CaO with the highest proportion in the slag used in this work (Table 1) will release a large number of Ca^{2+} and O^{2-}. In this case, Ca^{2+} and O^{2-} have much higher concentration than the other ions and thus they possess faster penetration rate with greater driving force. On one hand, when CA_6 in SII-10 comes into contact with the molten slag, it can react with Ca^{2+} and O^{2-} to form CA_2 according to Eq. (1). On the other hand, AlON can be oxidized by O^{2-}

ions to form more Al_2O_3 (Eq. (2)). These Al_2O_3 will further react with Ca^{2+} and O^{2-} to generate CA_2 as referred to Eq. (3). Based on this, the continuous and dense CA_2 is gradually form in corrosion zone, which can further improve the slag penetration and corrosion resistance of SII-10.

$$2Ca^{2+}_{slag} + 2O^{2-}_{slag} + CaAl_{12}O_{19matrix} \rightarrow 3CaAl_4O_7 \quad (1)$$

$$2Al_{23}O_{27}N_{5matrix} + 15O^{2-}_{slag} \rightarrow 23Al_2O_3 + 5N_2 \quad (2)$$

$$Ca^{2+}_{slag} + O^{2-}_{slag} + 2Al_2O_3 \rightarrow CaAl_4O_7 \quad (3)$$

Conclusions

In this work, CA_6/AlON composites with different amounts of AlON addition have been prepared using one-step and two-step methods, respectively. The phase distribution using two-step method is far more uniform. Furthermore, the optimized amount of AlON addition is 10 wt% (SII-10), in which the bulk density and apparent porosity are 2.26 g•cm^{-3} and 20.2%, respectively. In view of the slag penetration and corrosion test, the addition of AlON decreases the wettability of CA_6/AlON composites with the molten slag to a great extent. In addition, AlON oxidized by O^{2-} ions released from the molten slag can form Al_2O_3, which can further react with Ca^{2+} and O^{2-} ions to form dense and continuous CA_2 layer. This layer can effectively inhibit the further penetration and corrosion of molten slag.

Declarations

Acknowledgements

Yunsong Liu and Enhui Wang contributed equally to this work. This work was supported by the National Science Fund for Distinguished Young Scholars (No. 52025041), the National Natural Science Foundation of China (No. 51904021, 51974021), and the Fundamental Research Funds for the Central Universities (No. FRF-TP-19-008A1, No. FRF-TP-19-004B2Z), the project of Liaoning Province's "Rejuvenating Liaoning Talents Plan" (XLYC1902092) and Beijing Excellent Talents Foundation for financial support.

References

1. Chen JH, Chen HY, Mi WJ, *et al.* Substitution of Ba for Ca in the Structure of $CaAl_{12}O_{19}$. *J Am ceram Soc* 2017, **100**: 413-418.
2. Dong BB, Yuan B, Wang G, *et al.* Fabrication of porous SiC/calcium hexaluminate composites. *J Eur Ceram Soc* 2016, **36**: 3889-3893.

3. Xu LC, Wang EH, Hou XM, *et al.* Effect of incorporation of nitrogen on calcium hexaaluminate. *J Eur Ceram Soc* 2020, **40**: 6155-6161.
4. Li B, Li GQ, Chen HY, *et al.* Physical and mechanical properties of hot-press sintering ternary CM_2A_8 ($CaMg_2Al_{16}O_{27}$) and $C_2M_2A_{14}$ ($Ca_2Mg_2Al_{28}O_{46}$) ceramics. *J Adv Ceram* 2018, **7**: 229-236.
5. Utsunomiya A, Tanaka K, Morikawa H, *et al.* Structure refinement of $CaO{\cdot}6Al_2O_3$. *J Solid State Chem* 1988, **75**: 197-200.
6. Domínguez C, Chevalier J, Torrecillas R, *et al.* Microstructure development in calcium hexaluminate. *J Eur Ceram Soc* 2001, **21**: 381-387.
7. Iyi N, Takekawa S, Kimura S. Crystal chemistry of hexaaluminates: β-alumina and magnetoplumbite structures. *J Solid State Chem* 1989, **83**: 8-19.
8. Salomão R, Ferreira VL, de Oliveira IR, *et al.* Mechanism of pore generation in calcium hexaluminate (CA_6) ceramics formed in situ from calcined alumina and calcium carbonate aggregates. *J Eur Ceram Soc* 2016, **36**: 4225-4235.
9. Asmi D, Low IM. Physical and mechanical characteristics of *in-situ* alumina/calcium hexaluminate composites. *J Mater Sci Lett* 1998, **17**: 1735-1738.
10. Vázquez BA, Pena P, De Aza AH, *et al.* Corrosion mechanism of polycrystalline corundum and calcium hexaluminate by calcium silicate slags. *J Eur Ceram Soc* 2009, **29**: 1347-1360.
11. Xu L, Chen M, Wang N, *et al.* Corrosion mechanism of $MgAl_2O_4$-$CaAl_4O_7$-$CaAl_{12}O_{19}$ composite by steel ladle slag: effect of additives. *J Eur Ceram Soc* 2017, **37**: 2737-2746.
12. Feng B, Wang Z, Fan Y, *et al.* Creep deformation behavior during densification of ZrB_2-SiBCN ceramics with ZrO_2 *J Adv Ceram* 2020, **9**: 544-557.
13. Yao SZ, Wang EH, Chen JH, *et al.* Effectively controlling the crystal growth of Cr_2O_3 using SiO_2 as the second phase. *J Am ceram Soc* 2019, **102**: 2187-2194.
14. Luo Q, Gu H, Fang Y, *et al.* Enhancement of the densification and thermal properties of $Ca_2Mg_2Al_{28}O_{46}$ ceramic by MnO addition. *Ceram Int* 2020, **46**: 18734-18741.
15. Xu L, Chen M, Jin LY, *et al.* Effect of ZrO_2 addition on densification and mechanical properties of $MgAl_2O_4$-$CaAl_4O_7$-$CaAl_{12}O_{19}$ *J Am Ceram Soc* 2015, **98**: 4117-4123.
16. Corbin ND. Aluminum oxynitride spinel: A review. *J Eur Ceram Soc* 1989, **5**: 143-154.
17. Zhong X, Zhao H. High-temperature properties of refractory oxide-nonoxide composites. *China's Refract* 1999, **8**: 3-8.
18. Hong Y, Li Y, Tong SH, *et al.* Effect of the addition of Al powder on the microstructure and phase constitution of magnesia-spinel composites sintered at 1800 °C in N_2. *Key Engineering Materials* 2016, **697**: 345-349.
19. Takeda K, Hosaka T. Characteristics of new raw material alon for refractories. *Interceram* 1989, **38**: 18-22.

20. Ma C, Li Y, Jiang P, *et al.* Formation mechanism of γ-AlON and β-SiC reinforcements in a phenolic resin-bonded Al-Si-Al_2O_3 composite at 1700 °C in flowing N_2. *J Mater Sci* 2020, **55**: 5772-5781.
21. Murakami K, Iwasaki A, Akatsuka Y, *et al.* One results of sliding nozzle refractories using aluminum oxynitride. *Taikabutsu*
22. Hosaka T, Kato M. A study of compositional modification of trough mixture by using aluminum oxinitride. *Refractories* 1985, **37**: 22-26.
23. Sun WY, Yen TS. Phase relationships in the system Ca-Al-O-N. *Mater Lett* 1989, **8**: 150-152.
24. Zhang N, Liang B, Wang XY, *et al.* The pressureless sintering and mechanical properties of AlON ceramic. *Mat Sci Eng-A* 2011, **528**: 6259-6262.
25. Wang Y, Xie X, Qi J, *et al.* Two-step preparation of AlON transparent ceramics with powder synthesized by aluminothermic reduction and nitridation method. *J Mater Res* 2014, **29**: 2325-2331.
26. Su M, Zhou Y, Wang K, *et al.* Highly transparent AlON sintered from powder synthesized by direct nitridation. *J Eur Ceram Soc* 2015, **35**: 1173-1178.
27. Rodríguez-Galicia JL, De Aza AH, Rendón-Angeles JC, *et al.* The Mechanism of corrosion of MgOCaZrO_3-calcium silicate materials by cement clinker. *J Eur Ceram Soc* 2007, **27**: 79-89.
28. Kim NH, Fun QD, Komeya K, *et al.* Phase reaction and sintering behavior in the pseudoternary system AlN-Y_2O_3-Al_2O_3. *J Am Ceram Soc* 2005, **79**: 2645-2651.
29. Yan M, Li Y, Li H, *et al.* Preparation and ladle slag resistance mechanism of MgAlON bonded Al_2O_3-MgAlON-$Zr_2Al_3C_4$-$(Al_2CO)_{1-x}(AlN)_x$ *Ceram Int* 2019, **45**: 346-353.

Figures

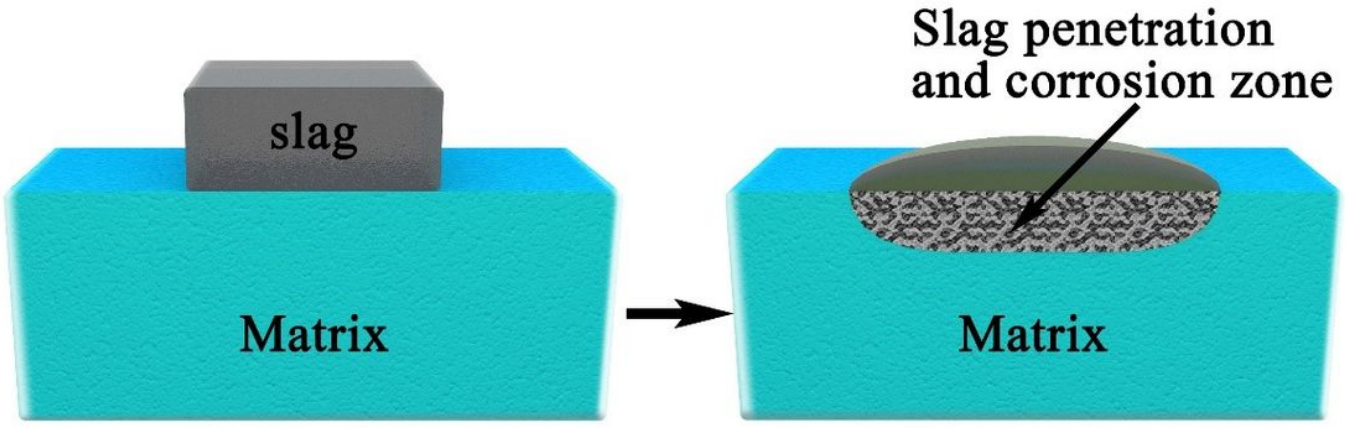

Figure 1

Shematic diagram of slag-matrix interface in the reaction test method

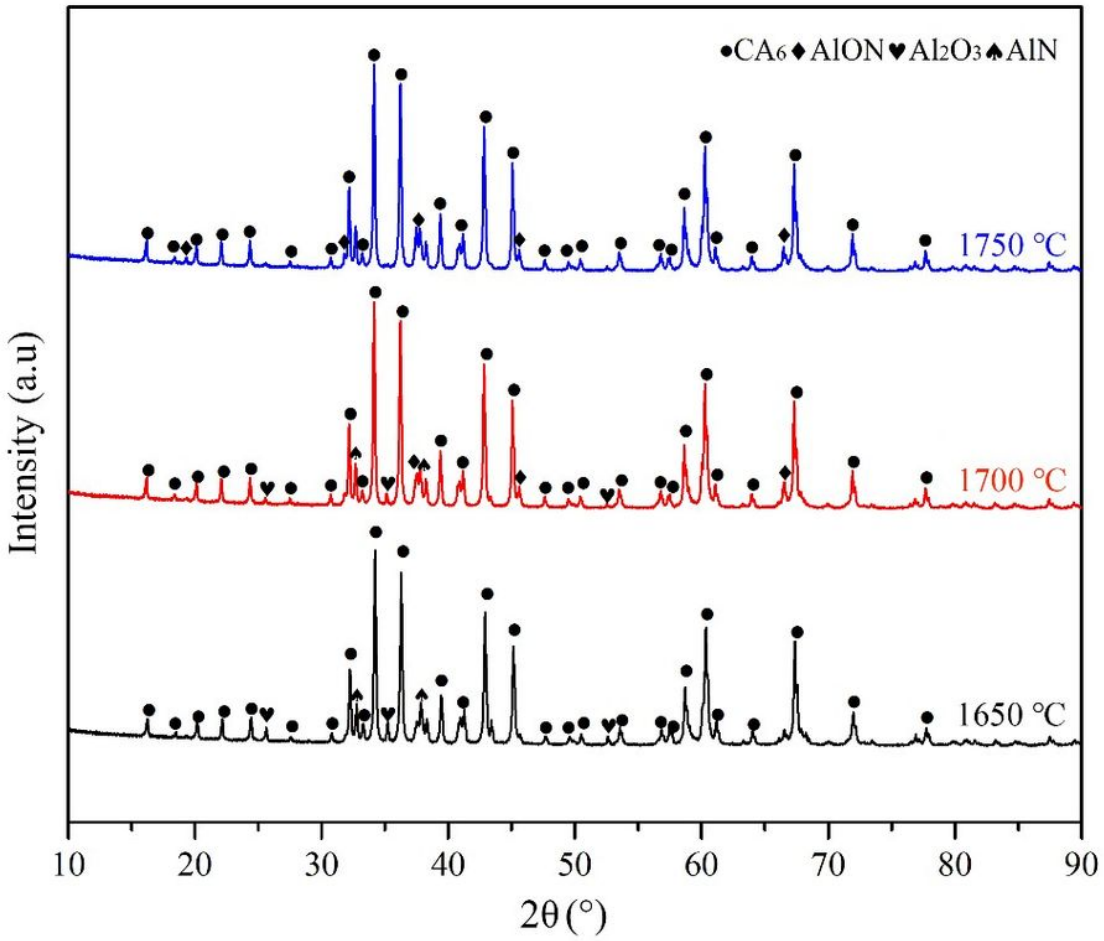

Figure 2

XRD patterns of SI-10 sintered at different temperatures for 3 h using one-step method.

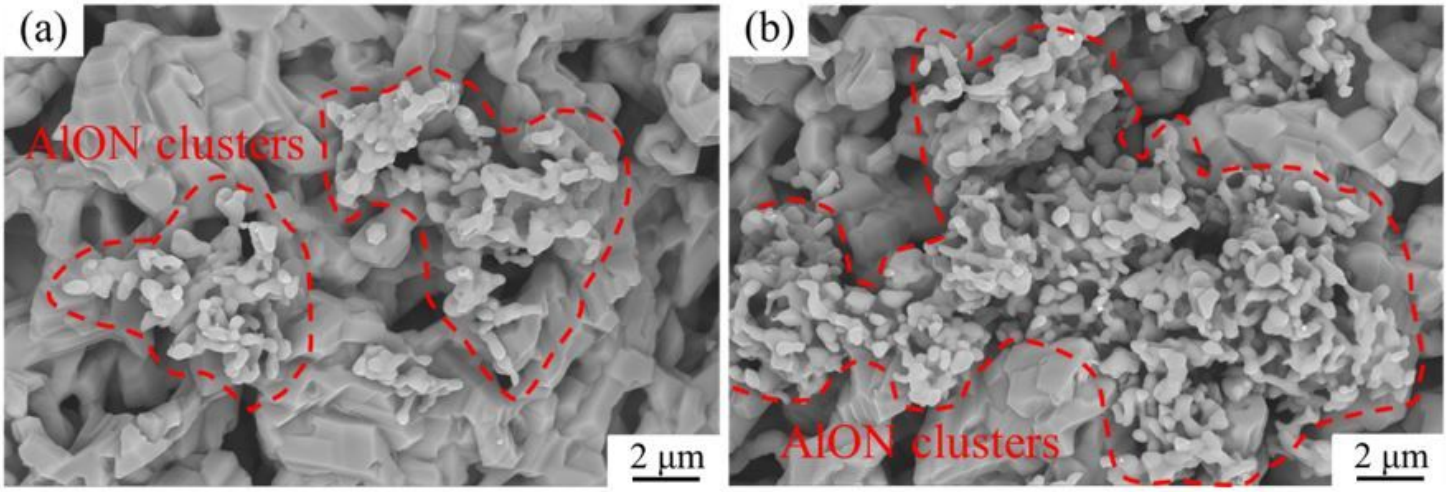

Figure 3

Typical fracture SEM images of (a) SI-10 and (b) SI-20 sintered at 1750 °C for 3 h using one-step method

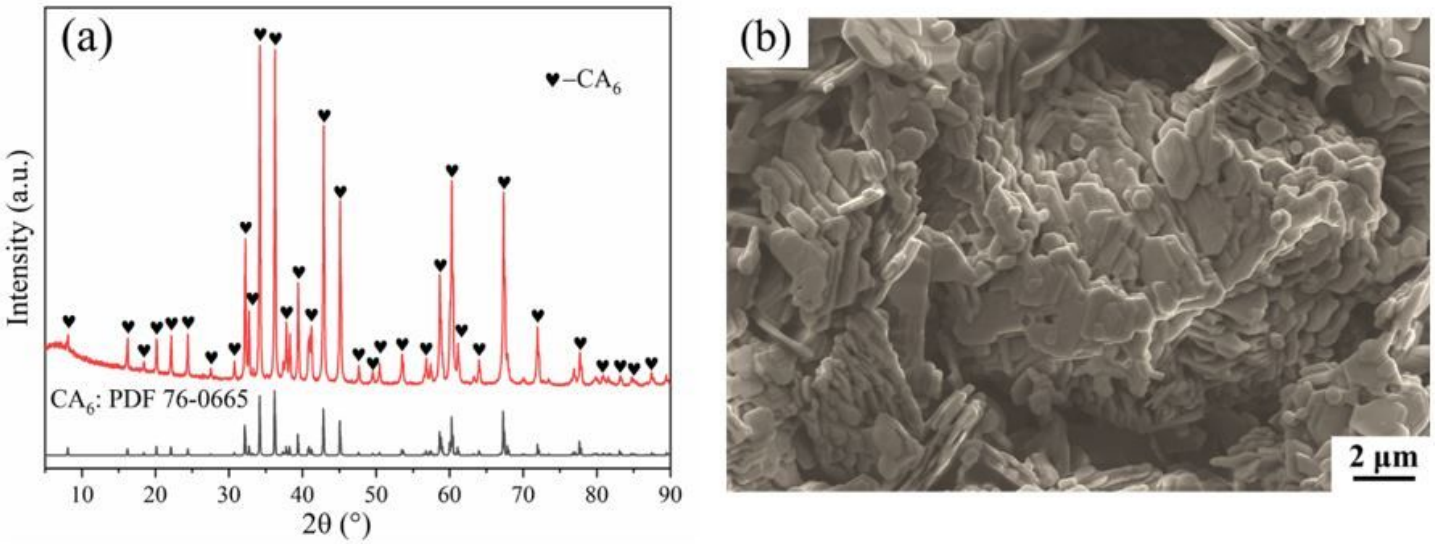

Figure 4

XRD pattern (a) and SEM image (b) of fracture CA6 sintered at 1550 ℃ for 2 h in air

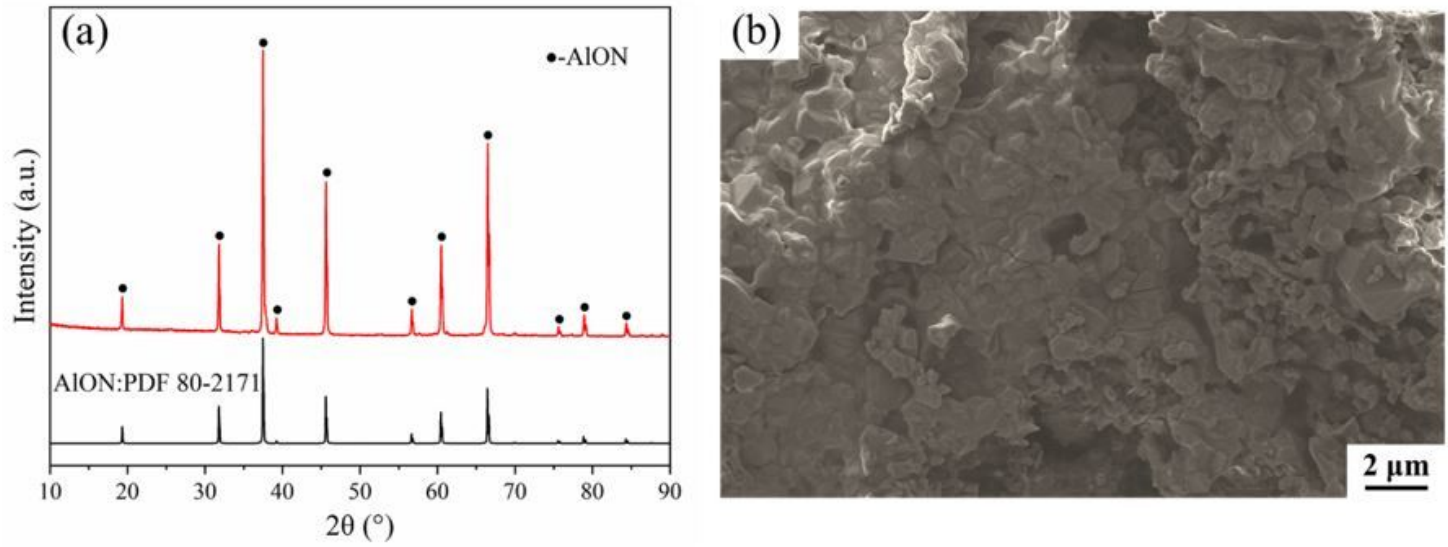

Figure 5

XRD pattern and SEM image of the fracture AlON sintered at 1750 ℃ for 2 h in flowing nitrogen atmosphere

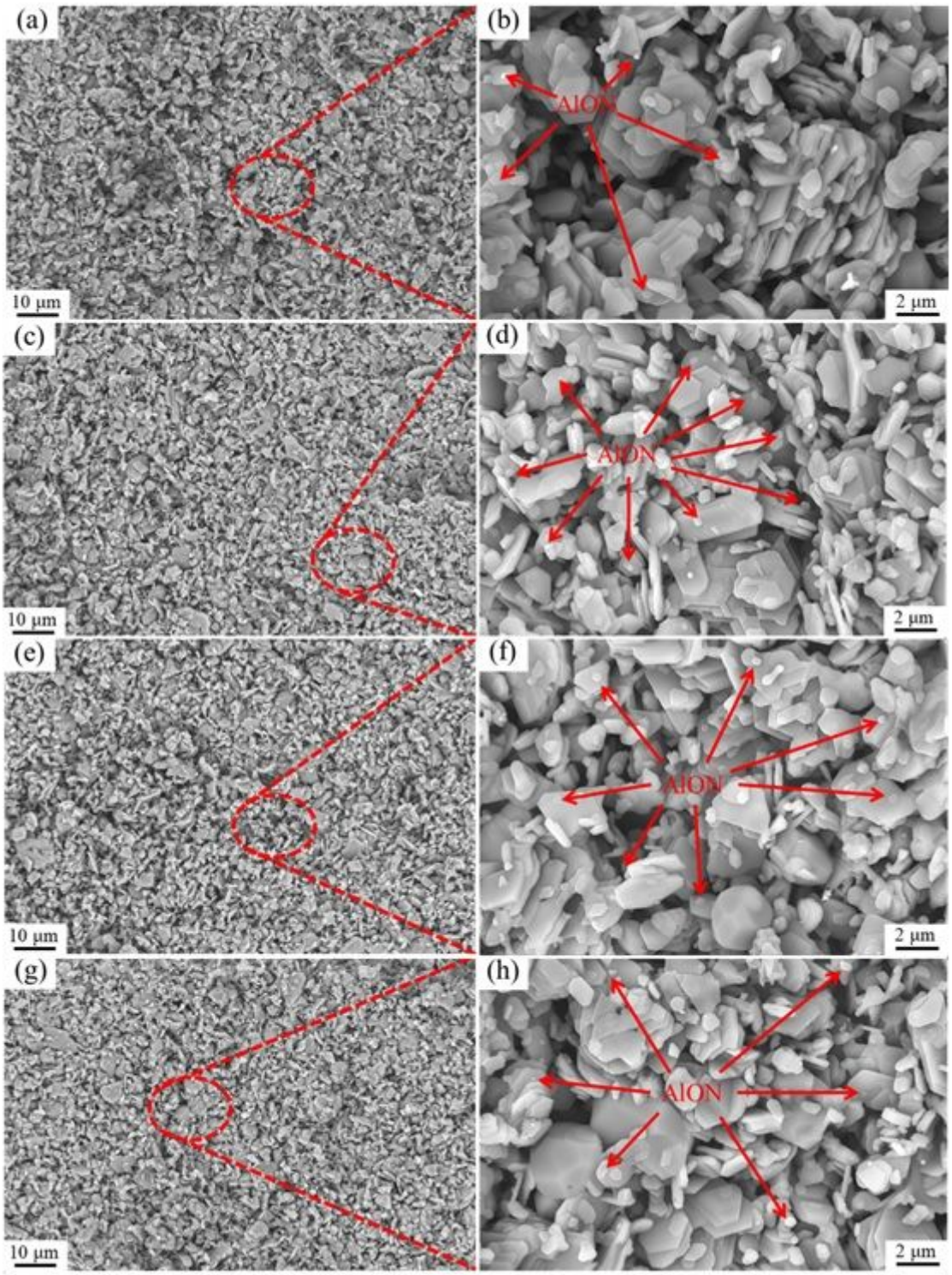

Figure 6

SEM images of fracture CA6/AlON composites with different amounts of AlON addition sintered at 1650 °C for 2 h: (a) SII-5; (c) SII-10; (e) SII-15; and (g) SII-20. (b), (d), (f) and (h) are local enlarged views of (a), (c), (e) and (g), respectively.

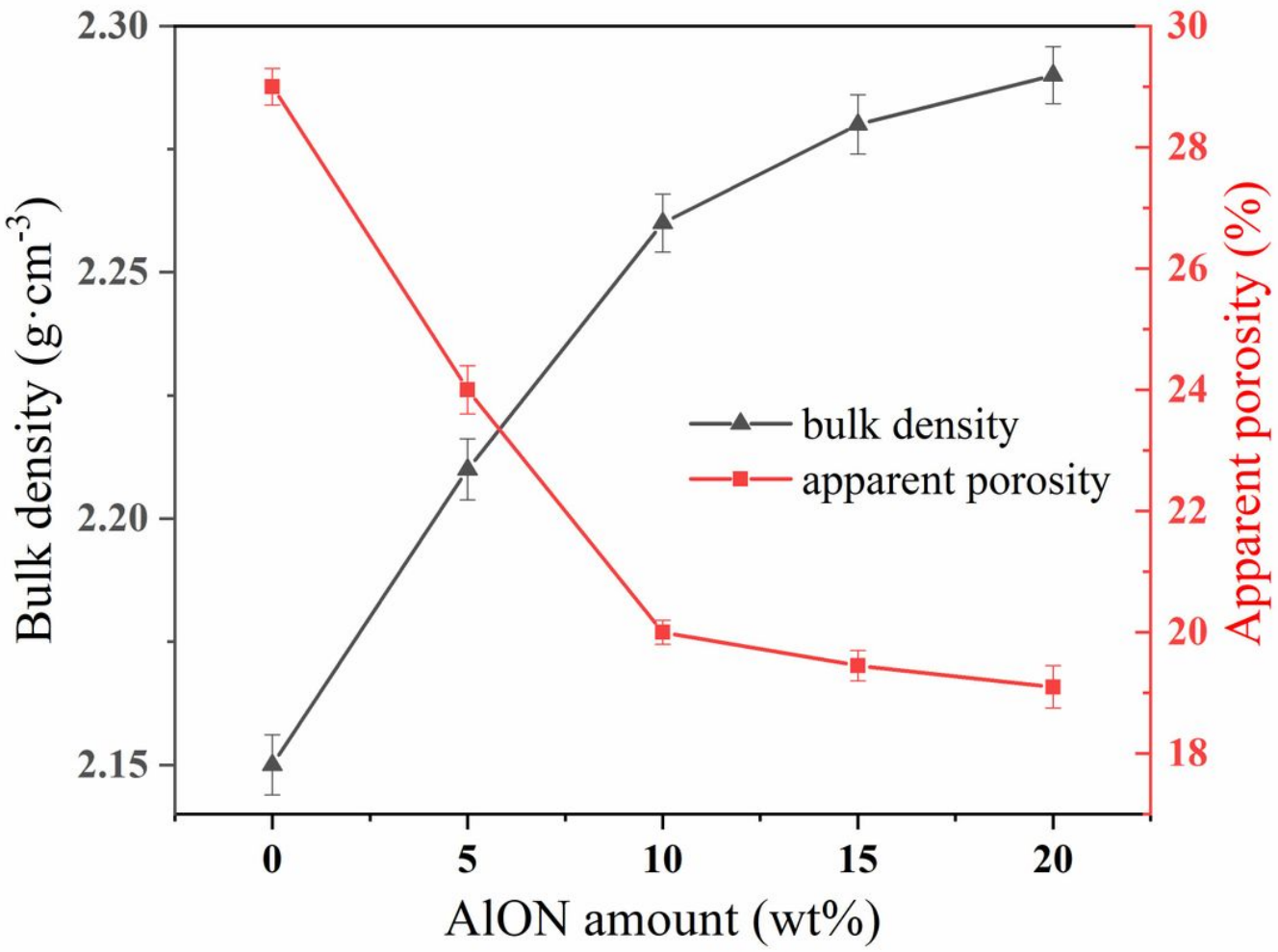

Figure 7

Bulk density and apparent porosity of CA6/AlON composites with different amounts of AlON addition prepared by two-step method

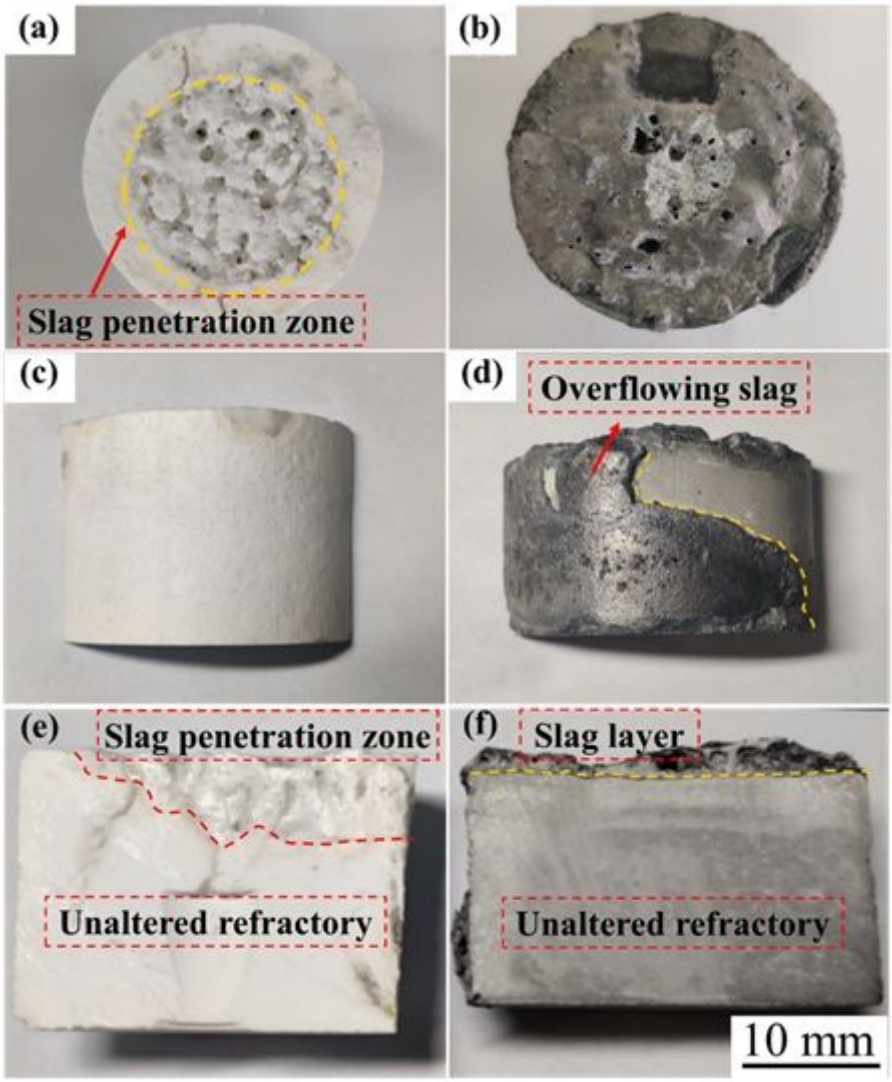

Figure 8

The top, left and cross-section views of pure CA6 and SII-10 after slag penetration and corrosion test in a buried carbon atmosphere at 1550 °C of 0.5 h: (a), (c) and (e) for pure CA6; (b), (d) and (f) for SII-10.

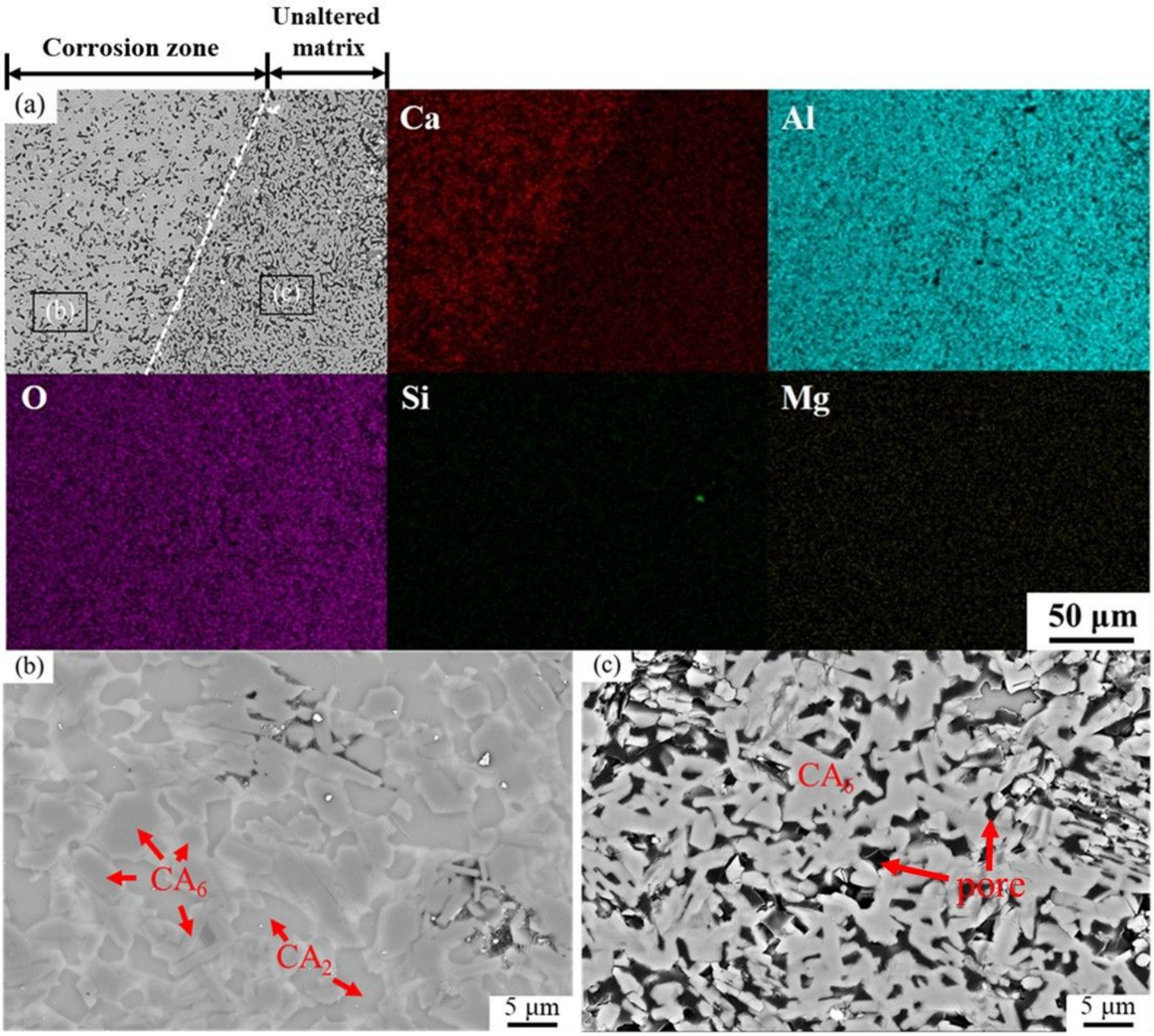

Figure 9

BSE images and corresponding element distributions of cross sections of pure CA6 sample after the slag penetration and corrosion test

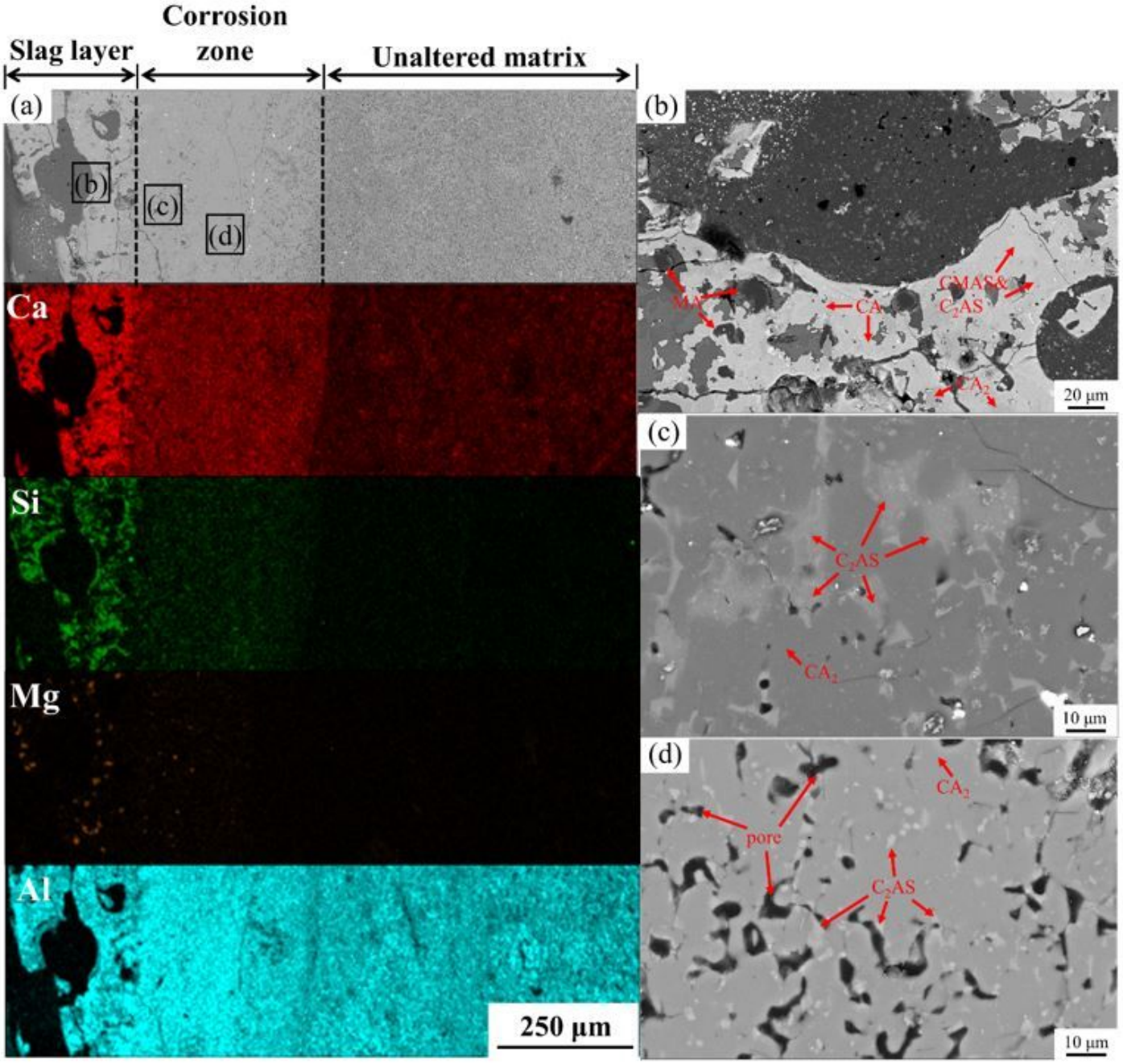

Figure 10

BSE images and corresponding element distributions of cross sections of SII-10 after the slag penetration and corrosion test